Lab on a Chip

Accepted Manuscript

This article can be cited before page numbers have been issued, to do this please use: A. Tayagui, Y. Sun, D. Collings, A. Garrill and V. Nock, *Lab Chip*, 2017, DOI: 10.1039/C7LC00725F.

ROYAL SOCIETY OF CHEMISTRY

rsc.li/loc

View Article Online
DOI: 10.1039/C7LC00725E
ROYAL SOCIETY OF CHEMISTRY

Journal Name

ARTICLE TYPE

Cite this: DOI: 10.1039/xxxxxxxxxx

An elastomeric micropillar platform for the study of protrusive forces in hyphal invasion†

Ayelen Tayagui,[ab] Yiling Sun,[a] David A. Collings,[c] Ashley Garrill,[b] and Volker Nock*[a]

Received Date
Accepted Date

DOI: 10.1039/xxxxxxxxxx

www.rsc.org/journalname

Oomycetes and fungi are microorganisms whose pathogenic (invasive) growth can cause diseases that are responsible for significant ecological and economic losses. Such growth requires the generation of a protrusive force, the magnitude and direction of which involves a balance between turgor pressure and localised yielding of the cell wall and the cytoskeleton. To study invasive growth in individual hyphae we have developed a Lab-on-a-Chip platform with integrated force-sensors based on elastomeric polydimethylsiloxane (PDMS) micro-pillars. With this platform we are able to measure protrusive force (both magnitude and direction) and hyphal morphology. To show the usefulness of the platform, the oomycete *Achlya bisexualis* was inoculated and grown on a chip. Growth of individual hyphae into a micro-pillar revealed a maximum total force of 10 μN at the hyphal tip. The chips had no discernible effect on hyphal growth rates, but hyphae were slightly thinner in the channels on the chips compared to those on agar plates. When the hyphae contacted the pillars tip extension decreased while tip width increased. *A. bisexualis* hyphae were observed to reorient their growth direction if they were not able to bend and effectively grow over the pillars. Estimates of the pressure exerted on a pillar were 0.09 MPa, which given earlier measures of turgor of 0.65 MPa would indicate low compliance of the cell wall. The platform is adaptable to numerous cells and organisms that exhibit tip-growth. It provides a useful tool to begin to unravel the molecular mechanisms that underlie the generation of a protrusive force.

1 Introduction

Over the past few decades, diseases caused by oomycetes and fungi have led to some of the most devastating die-offs and extinctions of flora and fauna ever witnessed, and this is a trend that is predicted to continue[1]. Numerous genera including *Phytophthora*, *Puccinia*, *Magnaporthe*, *Fusarium*, *Aspergillus*, *Nosema*, *Geomyces*, *Batrachochytrium* and *Candida* pose significant current threats to plants and animals. Furthermore, pathogenic species are becoming more widespread with increased dispersal due to modification of natural environments by human activity[2]. This will likely have profound effects on biodiversity, human and ecosystem health, and well being[1]. There are also significant economic implications as annual crop losses due to rusts, mildews and blights are a major problem around the globe, accounting for billions of dollars in lost productivity[3].

Oomycetes and fungi grow by a process called tip growth, which is characterised by extension at the apex of the cell. This is a complex process involving a turgor pressure and localised tip yielding, which leads to the formation of cylindrical cells or hyphae[4]. A key aspect of the pathogenicity of oomycetes and fungi is the ability of hyphae to grow invasively (i.e. through host tissue). Invasive growth is likely to involve enzymatic breakdown of host tissue and a protrusive force exerted by the hyphae[4]. The latter is likely to arise due to turgor pressure and increased yielding (through lessened resistance) of the tip to that pressure. Increased yielding in both oomycetes and fungi is thought to come about through modifications to both the cell wall and the cytoskeleton[5,6].

In general, advances in microfabrication and live-cell imaging mean that microfluidic devices are increasingly being used to study the forces that guide cellular processes[7]. Traditionally, such devices have been used extensively to measure mechanical forces related to mammalian cells[8,9]. More recently, Lab-on-a-Chip (LOC) technology has begun to be adapted for use with tip-growing organisms[10]. This includes the measurement of mechanical forces in fission yeast cells[11], the study of maze solving and dynamic behavior of basidiomycetous fungi[12,13], and the study of contact-induced apical asymmetry in the thigmotropic responses of *Candida albicans*[14,15]. More advanced devices have

[a] *Biomolecular Interaction Centre, Department of Electrical and Computer Engineering, University of Canterbury, New Zealand. Fax: +64 3 364 2761; Tel: +64 3 364 2987; E-mail: volker.nock@canterbury.ac.nz*
[b] *School of Biological Sciences, University of Canterbury, New Zealand.*
[b] *School of Environmental and Life Science, University of Newcastle, Australia.*
† Electronic Supplementary Information (ESI) available. See DOI: 10.1039/b000000x/

View Article Online
DOI: 10.1039/C7LC00725F

been employed to quantify the Young's modulus of primary plant cell walls[16], characterize the 3D morphology and mechanics of developing plant cells[17–19], and perform high-throughput analysis of single cell polarized growth and dynamics[20,21]. Until now, most measurements of protrusive forces have been made using substrates with a calibrated stiffness (e.g. agarose), waveguide sensors, optical traps and cantilevers, which have been placed in front of an advancing tip[22–24]. Of these techniques, micro-strain gauge cantilevers have proven to be most suitable given the magnitude of the forces to be measured. However, the strain gauge technique risks underestimating the effective force because of a shape change in the cell with the orthogonal contact of the tip with the flat surface of the sensor. Because of this an alternative approach was developed for cells that can easily reorient their growth direction in response to a mechanical trigger[25]. Narrow openings made using LOC technology from materials with calibrated elasticity, such as polydimethylsiloxane (PDMS), were presented as obstacles to tip growing pollen tubes cultured on a chip[16]. Finite element modeling and measurement of the dilating force exerted normal to the gap wall were then used to deduce the penetration pressure.

A technically simpler approach to measure forces exerted by cells as they grow and move is through the use of elastomeric micropillar arrays[26]. Initially developed to study cellular traction forces, these pillar arrays can be adopted for use with microorganisms such as nematodes[27–29]. The micropillar-based approach typically combines optical tracking of a pillar top with a simple mechanical model to measure forces. Given the correct modifications these arrays are applicable to hyphal organisms and provide the capability to also determine the directionality of forces generated[29]. Using photolithographic miniaturization approaches, the pillar system can be tailored to the size appropriate for the hyphae of the organisms to be studied. Previous work by us has indicated the suitability of the pillars for force sensing with hyphae[30]. However, using open arrays of micropillars only squeezing forces could be recorded, as hyphal tips were observed to preferentially grow into inter-pillar spaces, as opposed to against the sensor pillars. Following on from these results, we observed for the first time that hypha can be made to directly interact protrusively with pillar arrays by using microfluidic channels for confinement[31]. Whilst successful in demonstrating that micropillars could be used to measure protrusive forces, these early devices only produced low numbers of protrusive interaction events and we have since improved hyphal confinement on-chip to significantly increased these.

In the current study, we thus present an optimized LOC platform with integrated elastomeric micropillars capable of measuring the magnitude and direction of protrusive force generated by tips of the hyphae of the oomycete *Achlya bisexualis*[32]. We describe the fabrication of the polydimethylsiloxane (PDMS) chips that reliably facilitate the measurement of force at the hyphal tips and the associated force measurement process. We further detail the culture of organisms on the chips, the growth rates and morphology of hyphae, as well as observed hyphal tip - pillar interactions and their corresponding force values. While not a pathogenic species itself, *A. bisexualis* provides a useful model system for use with LOC technology as its hyphae are large and, as such, can be reliably imaged and grown relatively quickly[32]. The resulting new sensor platform is unique in its simplicity and capability of being able to measure both magnitude and direction of protrusive forces exerted by individual hyphae.

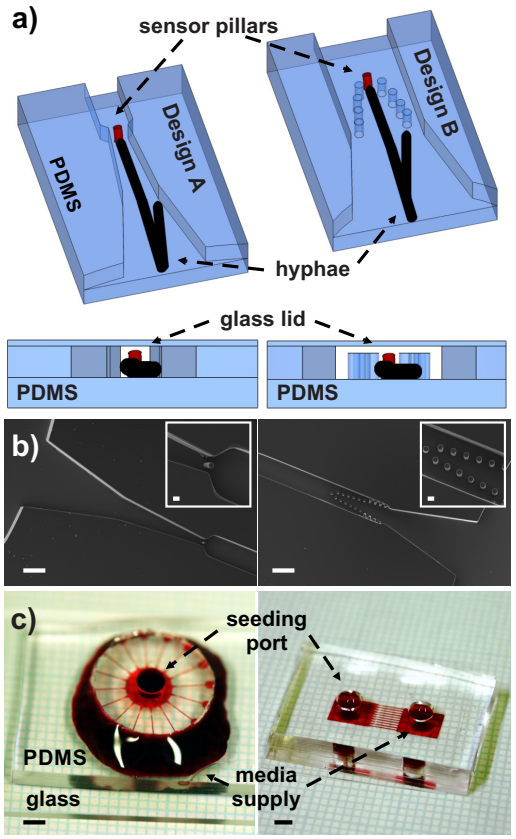

Fig. 1 Experimental setup. (a) Schematic of the measurement setup showing fungal hyphae growing into single (Design A, left) or arrays (Design B, right) of micro-pillars. Pillar deflection is recorded using an imaging setup and converted into force magnitude and direction. A glass lid, suspended above the pillar tops by the channel walls, is used to cover the devices. (b) Scanning-electron micrograph of the measurement area of the chips containing a single sensing pillar or pillar arrays inside a microchannel connected to a seeding area (Scale bar 50 μm). Insets show close-ups of the sensor pillars (Scale bar 10 μm). (c) Photographs of the two types of PDMS devices fabricated. The chip on the left incorporates 16 channels, while the device on the right contains 10 parallel channels, each with one measurement area per channel (Scale bars 2 mm). Red food-coloring is used to illustrate channels and ports.

2 Experimental

The design of the microfabricated devices is centered around cylindrical elastomeric micropillars located within rectangular microchannels. Hyphae grow against the measurement pillars and deflect these corresponding to the force applied, as shown in the schematic in Fig. 1(a). Pillars were used individually or in form of tapered arrays. Figure 1(b) shows scanning-electron micrographs (SEM) of the two pillar arrangements. Pillars were incorporated into two types of channel arrangements, with the measurement pillars located at constrictions 400 μm from the

View Article Online
DOI: 10.1039/C7LC00725F

channel entrance. The first configuration, shown on the left in Fig. 1(c), uses a star-like arrangement of 16 measurement channels. Originating from a large inlet port acting as a seeding area, channels initially taper to guide hyphae against either an array of pillars or a single pillar. Following the sensing area, channels continue with a constant width to individual outlets.

The second design, depicted on the right in Fig. 1(c), incorporates 10 parallel channels originating from the same inlet port and ending in the same outlet port. This design incorporates single measurement pillars and allows for the forces of multiple hyphae originating from the same mycelium to be studied in parallel under the same conditions. Both designs are microfabricated in PDMS and sealed using glass or PDMS lids containing drilled or punched access holes, respectively. These holes are used to seed the fungi and supply culture media. The dimensions of the measurement pillars were set to 25 μm height, and 7 μm and 10 μm for diameter. A horizontal gap of 10 μm separates the edge of the pillars from the channel walls. To allow the pillar tops to freely move for force sensing, channels were designed to be 30 μm deep, providing a 5 μm clearance gap from the top of the pillars to the channel glass lid.

Chip Fabrication

PDMS devices were fabricated using replica-molding of a two-layer resist master, as described in detail previously[28,30,31]. To guide hyphae against micropillars and enable control of the contact point, these pillars need to be confined inside microchannel constrictions. This geometry necessitates laterally confined, high-aspect ratio negative features on the mold master, which are difficult to reproduce in SU-8 negative resist[33]. In our previous work we overcame this difficulty by inverting the resist mold geometry and double-casting via an intermediate PDMS master[31]. However, this process exhibited a low pillar and device yield. For this work the process was thus modified to use a combination of negative and positive photoresists. By using thick positive resist instead of negative resist for the layer defining the measurement pillars, the optical problem of shadow-masking a high-aspect cavity inside a narrow channel is reversed into a lithographically simpler layout.

In brief, two 4" chrome-on-glass photomasks (Nanofilm) were prepared using a laser mask writer (uPG101, Heidelberg Instruments). The first layer mask contained the channel outlines and ports, while the second mask contained the same features plus the measurement pillars. Mask files used to produce the two devices are available in the ESI†. In parallel, a 5 μm thick negative-tone resist (ADEX5, DJDevcorp) was laminated onto a clean 4" silicon wafer using a hot-roll laminator (SKY335R6, Sky-Dsb Co.Ltd). Lamination was performed at 65 °C and speed 1 setting. The first layer mask was then exposed into the ADEX5 layer using a mask aligner (MA-6, Suss MicroTec) in vacuum contact mode. This was followed by a ramped post-exposure bake of 5 min at 65°C and 10 min at 95°C on a contact hotplate (HP30, Torrey Pines Scientific, Inc.). The wafer was developed in propylene glycol monomethyl ether acetate, rinsed with IPA and dried using N_2. A second layer of positive-tone photoresist (AZ40xT, M.M.R.C Pty Ltd.) was spin-coated onto the first layer to a thickness of 25 μm using a spin-coater (WS-650, Laurell). After edgebead-removal the resist was soft-baked for 3 min at 126°C on a hotplate and exposed using the second layer mask. This was followed by a post-exposure bake of 80 s at 105°C on a contact hotplate. Transferred patterns were developed by immersion into developer (AZ 326MIF, M.M.R.C Pty Ltd.) for 3 min, rinsed with DI water and dried using N_2.

Prior to PDMS casting the mold was treated for 2 h with trichloro(1H,1H,2H,2H-perfluorooctyl)silane (SigmaAldrich) in a vacuum to facilitate mold release. PDMS (Sylgard 184, Dow Corning) was mixed at 10:1 w/w ratio, degassed and poured onto the mold. After baking for 2 h at 80 °C on a hotplate, the cured PDMS was peeled off the mold and baked an additional 4 h at 80°C to ensure full hardening. PDMS covers were prepared by punching 3 mm holes into a flat piece of PDMS. Glass chip covers were prepared by drilling through-holes into standard 75 x 25 mm glass microscope slides (VWR) using a 3 mm diameter diamond-coated hole drill (28.5030, Esslinger). Both types of covers were manually aligned to the ports on the chips and bonded using 30 s exposure of both, the glass and PDMS, to 100 W oxygen plasma in a barrel asher (K1050X, Emitech). This was followed by a further bake of 2 h at 80°C on a hotplate to complete bonding. Fabricated PDMS chips were placed in a vacuum chamber and degassed for 2 h to prepare for vacuum-assisted filling[34]. Degassed chips were sealed into food-grade vacuum bags using a vacuum sealer (Sunbeam FoodSaver) and stored until use.

Oomycete Culture and Chip Loading

A female strain of the oomycete *A. bisexualis*, originally isolated from *Xenopus* dung and available from the University of Canterbury culture collection, was grown on peptone-yeast-glucose (PYG) agar plates (containing [in % w/v] Peptone [0.125], Yeast extract [0.125], Glucose [0.3], and Agar [2]). The surface of the agar was covered with sterile cellophane paper. Hyphae were grown for 48 h at 23.5 °C[5], after which an inoculation plug approximately 3 mm in diameter, was taken from the periphery of the culture and transferred to the PDMS chips. Prior to this, the chips were filled with PYG broth (containing [in % w/v]. Peptone [0.125]-Yeast extract [0.125] and Glucose [0.3]. In between transfer of Achlya onto the chip and when hypha entered the measurement area, fluid ports were regularly refilled with fresh broth to counteract evaporation. This was stopped as soon as hyphae approached the measurement area. Growth on the chips was monitored using a Nikon Eclipse 80i microscope at low magnification until hyphae had grown into the narrow channels towards the pillars. After this, the magnification was increased and observation was focussed on a/the pillar(s) of interest.

Force Sensing

The deflection of the pillar tops in contact with hyphae was recorded using an upright microscope (Nikon Eclipse 80i) and a digital camera (ORCA-Flash4.0 V2, Hamamatsu). Image acquisition was controlled by a PC running HCImageLive (Hamamatsu). The height of the contact point on the pillar was determined by focusing on the pillar top, re-focusing on the hyphal tip and recording the difference in micrometers on the microscope focus knob. Image sequences were imported into ImageJ (V1.51h, FIJI)[35], converted to 8-bit gray-scale format and pillar deflection was tracked using the TrackMate plugin (V3.4.2)[36]. Tracking out-

View Article Online
DOI: 10.1039/C7LC00725F

put from TrackMate was imported into MATLAB (2016a, Mathworks) and a custom script[27,28] was used in conjunction with pre-calibrated mechanical pillar properties[37] to convert the measured deflection into force magnitude and direction.

Growth-rate Characterization

To investigate any effect of the PDMS chips and channels on hyphal extension rate and morphology, growth rates and hyphal diameters 100 μm behind the tip were measured using the same microscope-based imaging setup as described above. Images of hyphae were processed in Photoshop (V6S, Adobe) and used to measure the growth rate and the hyphal diameter. These were compared to radial extension rates of colonies of hyphae that were growing on control PYG agar plates.

3 Results and discussion

Elastomeric micropillars were used as force sensors in this work to measure the protrusive force generated by tips of individual hyphae. Two different arrangements of measurement pillars, a single pillar placed at the narrowest point of a tapering microchannel (*Design A*) or a tapered array of 21 pillars inside a constant-width microchannel (*Design B*), were investigated. Narrowing of the channel in *Design A* prevented more than one hyphae reaching the measurement pillar. The second design allows for multiple hyphae to extend along the channel and for each to interact with individual pillars within the array. Both designs were incorporated into either a star-shaped or parallel channel arrangement. The former arrangement is based on the radial nature of the mycelium observed when grown on agar plates and offers the possibility to provide individualized stimuli to each of the channels.

Common to all chips produced for this work is that channels and measurement pillars are cast into a single monolithic piece of PDMS elastomer. After polymerization and cross-linking, solid PDMS presents an external hydrophobic surface[38], which may effect the growth rates of the organisms cultured on it. It has been shown that, for example, cell adherence and hyphae reorientation of *Candida albicans* hyphae grown on native and oxygen-plasma treated PDMS were reduced when compared to surface-modified PDMS[14]. In the devices presented here, PDMS constitutes the bottom surface and walls of the microchannels used to guide the hyphae, as well as the complete external surface of the measurement pillars. To better understand what influence this may have on organisms cultured within the device, we first measured the rate of growth of hyphae of *A. bisexualis* within the chip.

Hyphal Growth and Morphology

We analyzed the growth rates of *A. bisexualis* hyphae in the microchannels and compared these to radial extension rates of colonies of hyphae on PYG agar plates. Hyphae in the channels on the PDMS chips grew at an average rate of 6 + 1.6 μm/min (mean + S.D. (n=20)) in the channels, which was not significantly different (t-test) to the rate of 6.1 + 0.5 μm/min (mean + S.D. (n=5)) recorded measuring the radial extension on PYG agar Petri dishes. This suggests that the confines of the chip or the chip microenvironment had no effect on the growth rate. This is consistent with reports of tip growing pollen tubes, which grow at rates comparable to those in *in vivo* conditions[19]. Variable growth rates have been reported in the fungus *N. crassa*, although it should be noted that these were growing in very long channels and that channel length appeared to be the most crucial parameter in affecting growth rate[21]. Other works have described a slower rate of growth for *N. crassa* in spiral channels compared to wider channels[39]. Growth rates of oomycetes and fungi can be variable, typically ranging from 1 - 10 μm/min[40]). For the isolate of *A. bisexualis* used in the current study, rates around 6-8 μm/min have been previously reported[41], which is consistent with those observed on our platform.

Hyphae in the channels appeared healthy and displayed the usual characteristics of tip growth that are discernible with the light microscope (e.g. forward movement of the bulk cytoplasm with the extending tip and retrograde and anterograde movement of small refractile vesicles). Hyphal diameter, measured 100 μm behind the tips, was slightly narrower in the channels compared to PYG agar plates (21 + 2.2 μm (mean + S.D. (n=20)) compared to 24.9 + 2.7 μm (mean + S.D. (n=20)). The diameter of pollen tubes has also been reported to be influenced by the channel parameters with pollen tubes becoming thinner as they grew through channel constrictions[16]. While the hyphae in the present study were not growing through a constriction per se, it is likely that they are able to sense the geometry of the channel, given that hyphae of the dimorphic yeast *C. albicans* have been shown to alter their growth depending on the design of the channels on PDMS chips [14]. In previous work using an open array of pillars, and also in preliminary experiments with pillars and channels of different dimensions, we have observed that, if there was sufficient space between the pillar and the wall of the channel, hyphae have the ability to avoid the pillars altogether by reorienting their growth towards the gaps[30].

Force Sensing Principle

The protrusive force exerted by hyphae was measured via the deflection this force causes in a cylindrical micropillar made of elastic PDMS. This hypha-pillar contact force is collectively and equally loaded on the pillar, causing it to deflect as an elastic entity, similar to pillars used to measure forces exerted by nematodes[28]. Irrespective of the soft hyphal body, the force can be treated as a concentrated load at the center point of the contact area. Applying this force-deflection model, the total force f applied by the hypha corresponds to the total deflection of the pillar. Fluidic drag applied by the environment can be safely ignored[28] and no measurable adhesion force between the hyphal tip and pillar could be observed when tips disestablished contact. The deflection Δ of the free end of the pillar was recorded using a camera mounted on a microscope and measured using an open-source feature tracking algorithm[36]. A linear-spring force deflection model combining pure bending and shear[28]

$$f = \frac{\Delta}{(\frac{l^3}{3EI} + \frac{d^2(1+\gamma)l}{4EI}) + \frac{l^2}{2EI}(h-l)}, \quad (1)$$

where l is the contact height, I the moment of inertia, E and γ the Young's modulus and the Poisson's ratio for PDMS, respectively, and h the pillar height, was used to convert pillar deflection to force. A Poisson's ratio γ of 0.5 was used for PDMS[42]. The mo-

View Article Online
DOI: 10.1039/C7LC00725F

ment of inertia I in equation (1) is given by

$$I = \frac{\pi d^4}{64}, \tag{2}$$

where d is the diameter of the measurement pillar. For use with *A. bisexualis* we fabricated 25 μm high pillars with diameters of 7 and 10 μm. This equates to pillar aspect ratios of 3.6 and 2.5, respectively. Assuming hyphae with a width of 21 μm, these pillar dimensions equate to stiffnesses of 0.457 $\mu N/\mu m$ and 0.126 $\mu N/\mu m$, respectively. SEM imaging, as shown in Fig.1(b), confirmed that pillar diameters were uniform along the height. The Young's modulus E was determined to be 1.47 MPa using a set of calibration samples processed under the same thermal conditions as the devices described here. We used a piezoresistive force sensor setup to measure the Young's modulus, as described previously[37]. This value was confirmed using an electromechanical universal test systems (MTS Criterion - Model 43) using a 100 N load cell, MTS Testworks 4 software and MTS Videotraction to measure the strain. As *A. bisexualis* hyphae have a cylindrical body shape[32], it is assumed that a hypha applies force using its tip to the pillar at half its body height. To compensate for variations in hyphae, we manually measured the width of each hypha at a distance of 10 μm behind the hyphal tip using ImageJ. Half of this value was then used as the contact height l in equation (1). This was further confirmed by measuring the vertical distance between the top of the pillar and the hyphal tip at the moment of contact using the micrometer scale on the microscope focus dial. We estimate the precision of this approach to be +/- 1 μm, which equates to a force error of +/- 6.7%. In the future we are aiming to integrate side-viewing[43] into the chips.

Pillar Deflection Tracking

To track pillar deflection with sub-pixel accuracy, we used optical microscopy combined with the ImageJ particle tracking plugin TrackMate[36]. Hyphae were first visually tracked using optical microscopy at low magnification while they grew into the measurement channels. Figure 2(a) shows an example of *A. bisexualis* hyphae growing into the tapering microchannels leading off from the central seeding area on a star-shaped *Design A* chip. Once hyphal tips approached within 1 mm of the measurement pillar further extension was recorded using a 20x objective. Recorded image sequences were imported into ImageJ and the graphical user interface of TrackMate was used to define tracking parameters. First, a Laplacian of Gaussian (LoG) filter was applied with an estimated pillar diameter specified in pixels. Using the plugin interface, sub-pixel localization can be implemented by activating a quadratic fitting scheme and a threshold parameter can be used to further reduce the number of circles identified for tracking. Resulting circular features are overlaid onto the image sequence using the ImageJ hyperstack viewer after applying a suitable filter to limit tracking to only the pillar of interest. Figure 2(b) shows this step as close-up for the hypha in the top channel of Fig. 2(a) once it had reached the pillar. We used the built in simple Linear Assignment Problem (LAP) tracker and found this tracker very robust, even in the presence of debris close to the pillar, as evident in Fig. 2(b). This tracker allows one to specify maximum linking and gap-closing distances, which can be used to bridge discontinuities in the tracking due to misidentifications. As a final step, tracking data was exported in 2D coordinate/time (X,Y,t) format to an eXtensible Markup Language (XML) file. We also trialled a custom algorithm previously developed for the tracking of pillars actuated by *C. elegans*, which was based on least-squares circle detection[27,28]. However, this algorithm did not yield as satisfactory results as TrackMate, possibly due to the smaller size and larger pillar deflections observed in the current devices. Both these methods are ultimately limited by the ability to determine the position of the pillar top circle. At extreme deflections, for example caused by large diameter hyphae in combination with smaller diameter pillars, the tracking, and thus force measurement will only be successful for a certain period of time after contact. In fact, we have observed several larger diameter hyphae fully flattening smaller pillars after short periods of time. While a force measurement is still possible in such a case, a larger pillar diameter (larger stiffness) will need to be chosen should a longer measurement time be desired.

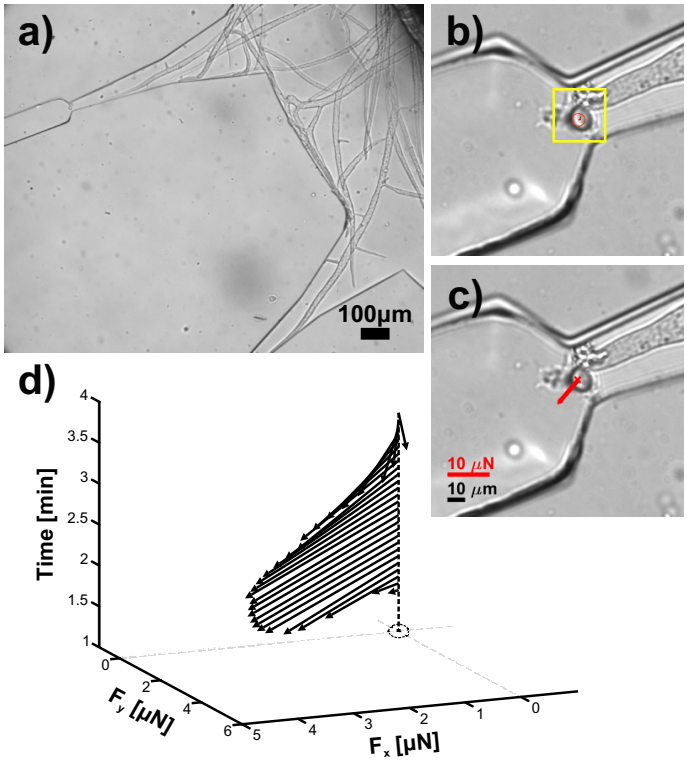

Fig. 2 Force sensing on individual hyphal tips. a) Optical micrograph showing hyphae growing out from a mycelial plug of *A. bisexualis* placed in the central seeding area. Hyphae grow radially outwards into the tapering measurement channels. Individual 10 μm diameter force sensing pillars are located at constrictions within each channel. b) Close-up of a sensing pillar at 30 s showing circle tracking data generated by TrackMate as red line. The box corresponds to an area-crop defined in ImageJ to reduce the number of features tracked. c) Force direction and magnitude overlay at the same time-point as in (b) generated using custom code in Matlab. d) Plot of the force vector of the hyphal tip - pillar interaction as a function of time. Both force magnitude and direction are recorded and can be related to contact phases.

Force Data Processing

Force vector data was generated from TrackMate output via

View Article Online
DOI: 10.1039/C7LC00725F

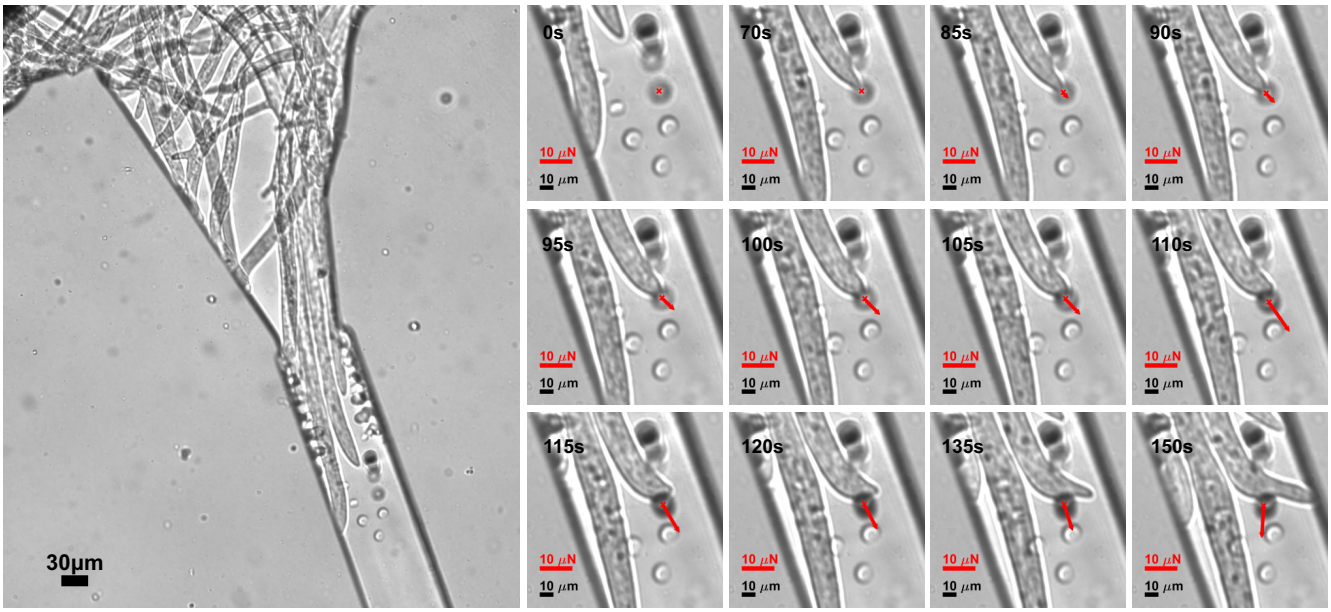

Fig. 3 Example of a hyphal tip - pillar interaction. Optical microscopy images of a set of hyphae growing into a microchannel towards a tapered array of measurement pillars. The time series shows an individual hypha interacting with one of the measurement pillars. Pillar tracking data output from Matlab is overlaid onto the images depicting pillar centre-point tracking (red cross) and force direction and magnitude (red vector). The hyphal tip can be observed extending towards the pillar, making contact and displacing the pillar. After the 105 s mark the hypha deflects off the pillar, as it is unable to penetrate, leading to a transition from protrusive to bending force.

custom code implemented as a MATLAB script. While it would be possible to implement some of this functionality via the ImageJ scripting language, this would ultimately not be as powerful as the use of a dedicated data analysis tool such as Matlab. The script itself contains the force model described in eq.(1) and allows one to input mechanical and geometrical properties, as well as calibrate image dimensions. Tracking data is imported via the ImageJ-Matlab extensions and converted to force values for each image in the sequence. These values are used to generate directional force vectors and overlay these onto the image files together with scale bars, as shown in Fig. 2(c). The overall output of the script includes individual frames, an animated movie of the sequence and force data as a text file and 2D and 3D force vs. time plots. Figure 2(d) shows an example of the force vector plot generated by the hypha shown in Fig. 2(c). Both magnitude and direction of the protrusive force exerted on the pillar are recorded. In this example, pillar contact and protrusive force generation are initiated 1.5 min after the recording starts. Over a period of 30 s, the x and y components of the force applied by the hypha can be seen to increase rapidly from 0 to 4.5 and 5.2 μN, respectively. After this, a gradual decrease in force components and a change of direction in the vector is observed, indicating that the hypha deflects to the right of the pillar. An example video showing hyphal extension into the channels and force measurement is available in ESI, Movie S1†.

In general, we have observed that smaller hyphae, after applying an initial protrusive force, will deflect off stiff (larger diameter) pillars, while larger hyphae will grow straight through (effectively over) softer (smaller diameter) pillars, bending these entirely flat in the process. The force resolution of this approach can be estimated using the product of the pillar stiffness, pixel size u in either direction and the visual tracking resolution σ. The pixel size was calibrated to be 0.47 x 0.47 μm and σ estimated to be 0.5 pixel[28]. From this follows that, for a pillar diameter of 10 μm and a hypha width of 25 μm the force resolution is 0.08 μN. This resolution increases to 0.02 μN if the pillar diameter is reduced to 7 μm for the same hyphal width. It should be noted that our current mechanical model does not take into account substrate warping, which has been found to systematically overestimate forces at low aspect ratios and low Poisson ratio[44]. Given that the pillar sensor is attached at one end (bottom of the channel) and free at the other end, a protrusive force in the z-direction may also be generated. However, all our observations to this date indicate that, if existent, this protrusive force in the z-direction would be very small compared to forces in the x- and y-directions, as optical micrographs and confocal imaging (data not shown) do not evidence vertical deflection while hyphae interact with the pillars.

Force Patterns in Hypha-Pillar Interactions

To demonstrate the capability of our platform we used the pillar arrays in Design B for investigations of the relationship between changes in hyphal growth, morphology and force generation. The spacing of the pillars in this arrangement allows for a hypha to contact individual pillars, apply force and subsequently move around them if the pillar stiffness is too large to allow the hypha to extend through the pillar. A representative hyphal tip - pillar interaction is shown in Fig. 3 as a series of optical micrographs. A video showing the complete hypha-pillar interaction and corresponding force measurement is available in ESI, Movie S2†. Measurements obtained from this series of images are shown in Fig. 4. On the left in Fig. 3 multiple hyphae can be seen entering the pillar array area of the channel. One of these

View Article Online
DOI: 10.1039/C7LC00725F

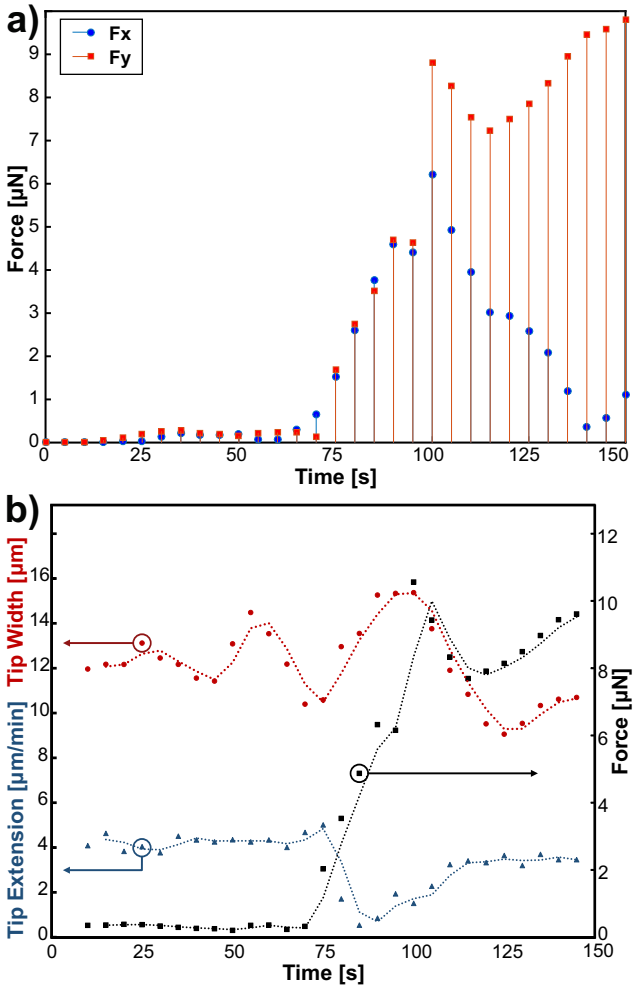

Fig. 4 Results of a typical hyphal tip - pillar interaction. a) Plot of measured force components in the x- and y-direction as a function of time. Directional changes can be observed as the tip goes through different stages of interaction. b) Comparison of the total force and related hyphal parameters, tip width and extension, as a function of time. Tip extension was measured as a change of tip position along the current orientation of the tip between frames.

hyphae grows towards a single pillar and begins to interact with it at the 70 s mark. Firstly, within seconds upon contact, an increase in pillar deflection and thus force is visible. The length of the force vector increased steadily and remained pointing in the same direction. A plot of the extracted x-and y-components of the protrusive force, as shown in Fig. 4(a), indicates a steady increase of both components initially while the hyphae increases force generation. Starting from the same time-point, changes in hyphal extension could also be observed as the tip began to interact with the pillar. From the onset of protrusive force generation at 70 s, the hypha appeared to slow down. This behavior was confirmed in the measured extension rate, which was relatively constant prior to contact with the pillar, but was observed to decline from 4 μm/min to less than 1 μm/min in Fig. 4(b) as it contacted the pillar.

During the same period the diameter of the hypha visibly increased. Again, we were able to confirm this by measuring of the width of the hypha 10 μm behind the tip. As shown in Fig. 4(b), there was an increase in hyphal width from 12 μm to 15 μm during this period. After approximately 100 s, the tip of the hyphae can be seen to change direction and, through images 105 s to 135 s, extend past the pillar. Similar contact-induced behavior has also been observed in *Candida albicans* hyphae growing against PDMS obstacles[14]. For *C. albicans* it was concluded that hyphal reorientation occurs at tip pressures higher than those required for plasma membrane penetration. The change in direction of *A. bisexualis* also corresponds with a change from protrusive to squeezing force, a momentary drop in total force and reduction of pillar width, as illustrated in Fig. 4(b). Simultaneously, the tip extension rate can be seen to recover to close to its pre-contact value over the same period. This demonstrates that force measurement on the platform can be combined with observations of changes in hyphal growth rates and morphology. Published micrographs of hyphae growing into micro-strain gauges suggest that the *A. bisexualis* hyphae widen subapically as they make contact with the gauge[45].

In addition to understanding force patterns, the measurements we have made of protrusive forces can also used as an indication of the compliance of the cell wall. If one considers the x and y components of the force applied by the hypha at 90 s in Fig. 4(a), 4.6 and 4.8 μN, respectively, this would give a total force of 6.7 μN. Given a hyphal diameter at the point of contact of 7 μm and assuming that the point of contact is circular, the area of contact with the pillar at the time of measurement can be estimated to be 77 μm^2. This translates into a total pressure during contact of approximately 0.09 MPa. We have previously reported turgor values of 0.65 MPa when *A. bisexualis* is grown in PYG media[46]. As a consequence, this suggests that just 14 percent of the turgor pressure is generating protrusive force and the rest must presumably be overcoming wall/cytoskeletal resistance, indicating low compliance of the cell wall. This is consistent with the findings of others who have measured protrusive force in hyphae using a micro-strain gauge. For *A. bisexualis* pressures of 0.11 MPa were exerted by hyphae with measured turgor pressures of 0.69 MPa[47], thus only 16 percent of turgor was generating protrusive force at the tip. For other oomycete species values ranged from 2 percent to 54 percent, with the higher value only observed under certain conditions, and for fungi values ranged from 9 percent to 32 percent[47]. These values contrast with those from tip growing pollen tubes, where the maximum pressure exerted on the sides of a micro-gap in channels was 0.15 MPa. In pollen tubes typical turgor pressures of between 0.2 MPa[16] up to 0.35 MPa[19] have been reported, suggesting a much more compliant cell wall, i.e. a much higher proportion of turgor is generating protrusive force rather than overcoming wall/cytoskeletal resistance.

As detailed above, we have also designed chips with parallel channels to investigate the possibility of the simultaneous measurement of force, growth rate and morphology in multiple hyphae (Fig. 1(c) (right)). These chips contain a total of ten channels originating from the same seeding area and terminate in a shared outlet. Channels are pre-filled with media and a mycelial plug is inoculated into the seeding area. During experiments media can be added to or removed from each port by pipetting. Figure 5(a) shows a lower magnification image of *A. bisexualis*

View Article Online
DOI: 10.1039/C7LC00725F

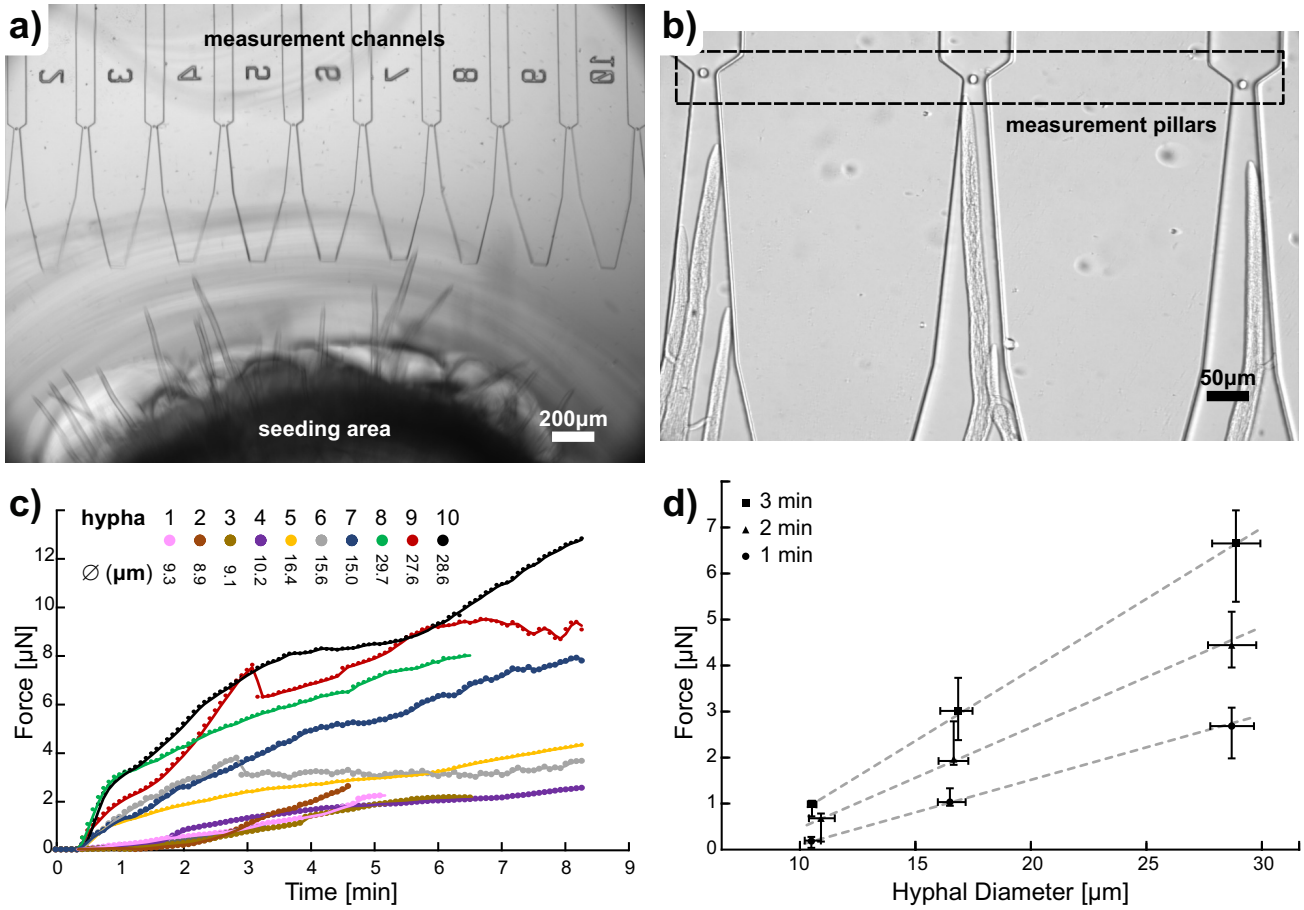

Fig. 5 Multiplexed force sensing. a) Low resolution optical micrograph of hyphal tips growing towards ten parallel measurement channels containing micro-pillars. Channels originate from the same seeding area and end in a shared outlet. Hyphae extend out of the same mycelial plug and grow into the parallel channels for measurement. b) Optical micrograph showing three hyphae extending towards measurement pillars on the chip. At the resolution required to reliably track pillar tops a maximum of three channels could be observed in parallel. The highlighted area indicates a top-view of the measurement pillars at the microchannel constrictions. The narrowing channel shape was chosen to prevent multiple hyphae from entering the measurement area and to stop branching close to the pillars. c) A plot of the total protrusive force exerted as a function of time by ten hyphae growing individually in separate measurement channels on the chip. Measured at a distance 10 μm behind the tip, individual hyphal diameters ranged from 8.9 μm to 29.7 μm and were observed to increase with time. For a period of 20 s upon hypha - pillar contact force values show a rapid increase, which is associated with protrusive force generation. After this period forces increase more gradually and correspond to a combination of squeezing and bending forces. d) Plot of the protrusive force of the same ten hyphae as a function of hyphal diameter measured at 1, 2 and 3 min after pillar contact. Both, hyphal diameter and generated protrusive force can be seen to increase.

hyphae extending towards the parallel measurement channels. Upon inoculation hyphae extended out of the mycelial plug and grew into the parallel channels. All ten channels can be observed simultaneously at this magnification. However, to reliably track the pillar tops for force sensing, the magnification has to be increased, thereby limiting concurrent measurement to three parallel channels. This limited field of view required for measurement does not significantly reduce the number of hyphae that can be observed on the same chips, mainly due to the fact that hyphae were observed to typically reach the central channels first, a behavior most likely due to the shorter distance from the mycelial plug. A video showing an example of measurement of protrusive force in the parallel channel chip is available in ESI, Movie S3†.

Three of these channels are illustrated in Fig. 5(b) with the measurement pillars highlighted in close proximity to three individual hyphae in each channel. To demonstrate the potential of this layout we have used the chip to compare force magnitudes and their progression in multiple hyphae. Figure 5(c) shows an example of the progression of total protrusive force as a function of time as applied by ten individual hyphae growing into pillars at the constrictions of parallel channels. Force curves were similar for the ten hyphae - for a period of around 20 s upon hypha-pillar contact force values rapidly increased, which is associated with protrusive force generation. After this period, forces increase more gradually and correspond to a combination of squeezing and bending forces. More noticeable was the difference in force magnitudes between individual hyphae.

Figure 5(d) demonstrates the types of direct comparisons possible with the parallel channel layout. In this example, the force generated by the hyphae is compared as a function of their diameter. Tracking of all ten hyphae showed a slight widening and an increase in force with contact time for each. However, most noticeable was that the force a hypha can generate appears to be directly related to its diameter. Smaller diameter hyphae (hy-

View Article Online
DOI: 10.1039/C7LC00725F

pha 1, 2, 3, 4; 9.3, 8.9, 9.1, 10.2 μm, respectively) appear to generate smaller force values than medium sized (hypha 5, 6, 7; 16.4, 15.6, 15.0 μm, respectively) and larger hyphae (hyphae 8, 9, 10; 29.7, 27.7, 28.6 μm, respectively). For all hyphae this force increases with time after initial contact, a trend which is also apparent in the individual force plots shown in Fig. 5(c). The capability to measure the force of hyphae with varying size without the need to change device layout is an inherent strength of the pillar-based platform and we are currently using this to perform in-depth studies into the influence of various hyphal parameters on force generation. While this size-independence is ultimately limited by the gap between the pillar and channel wall, which prevents hyphae from avoiding the pillar, down-scaling the platform to suit smaller species of hyphae and oomycetes is straight forward as far as photolithography and pillar tracking allow.

In addition to addressing questions related to wall compliance, the chips may also provide the means to concurrently measure protrusive force and observe the dynamics of the cytoskeleton with the use of appropriately transformed strains of oomycete or fungi[48]. Thus, direct investigations of the potential role of the cytoskeleton in modulating protrusive forces are possible. Furthermore, the use of a single cell pressure probe[5] may also enable the concurrent measurement of turgor pressure and force. As a result, we may now have in place the experimental tools and systems to better understand the mechanisms that enable fungi and oomycetes to grow invasively and cause disease. This understanding may impact on how we address the many diseases and infections that occur due to invasive fungal and oomycete growth and may enable us to combat further loss of biodiversity due to these organisms. An understanding of the molecular dynamics that underlie this mode of growth may provide additional means of stopping this growth and may enable us to combat further loss of biodiversity due to these organisms.

4 Conclusions

We have demonstrated the first use of elastomeric micro-pillar arrays for the study of protrusive forces in hyphal invasion. Devices containing pillar arrays for force measurement were fabricated using a double-layer resist mold and PDMS soft-lithography. Following plasma treatment, growth media was introduced into the devices and *Achlya bisexualis* was seeded as mycelial plugs. Growth was monitored on-chip and occurred at a comparable rate to growth on PYG agar media. Hyphae were observed to grow into micro-pillar arrays. Force measurements and hyphal-pillar interaction studies were performed by recording pillar deflection and optical tracking of hyphal widths and extension rates. Tip extension was found to decrease and tip width to increase during pillar interaction and protrusive force generation. *A. bisexualis* hyphae were observed to reorient at tip pressures higher than those required for plasma membrane penetration. Measured force magnitudes and directions were converted into pressures and were comparable to those generated using existing methods, showing good agreements. Total forces ranging from 0.5 to 10 μN were measured, with forces typically increasing as a function of hyphal diameter and contact time. The current platform provides a useful tool to study the molecular mechanisms enabling protrusive force and may help to address the many diseases and infections that occur due to invasive fungal and oomycete growth.

5 Acknowledgements

The authors would like to thank Helen Devereux, Gary Turner and Kevin Stobbs for technical assistance. Financial support was provided by Marsden Grant UOC1504, the Brian Mason Trust and the Biomolecular Interaction Centre.

References

1 M. C. Fisher, D. A. Henk, C. J. Briggs, J. S. Brownstein, L. C. Madoff, S. L. McCraw and S. J. Gurr, *Nature*, 2012, **484**, 186–94.
2 D. P. Bebber, M. A. T. Ramotowski and S. J. Gurr, *Nature Clim. Change*, 2013, **3**, 985–988.
3 D. W. Denning, A. Pleuvry and D. C. Cole, *Eur. Respir. J.*, 2013, **41**, 621–626.
4 R. R. Lew, *Nat. Rev. Micro.*, 2011, **9**, 509–518.
5 S. K. Walker, K. Chitcholtan, Y. Yu, G. M. Christenhusz and A. Garrill, *Fungal. Genet. Biol.*, 2006, **43**, 357–365.
6 S. Suei and A. Garrill, *Protoplasma*, 2008, **232**, 165–72.
7 M. Eisenstein, *Nature*, 2017, **544**, 255–257.
8 W. J. Tyler, *Nat. Rev. Neurosci.*, 2012, **13**, 867–878.
9 T. Iskratsch, H. Wolfenson and M. P. Sheetz, *Nat. Rev. Mol. Cell Biol.*, 2014, **15**, 825–833.
10 C. E. Stanley, G. Grossmann, X. Casadevall i Solvas and A. J. deMello, *Lab Chip*, 2016, **16**, 228–241.
11 N. Minc, A. Boudaoud and F. Chang, *Curr. Biol.*, 2009, **19**, 1096–1101.
12 K. Hanson, D. Nicolau, L. Filipponi, L. Wang, A. Lee and D. Nicolau, *Small*, 2006, **2**, 1212–1220.
13 M. Held, M. Binz, C. Edwards and D. V. Nicolau, Proc. SPIE 7182, Imaging, Manipulation, and Analysis of Biomolecules, Cells, and Tissues VII, pp. 718213–718213–9.
14 D. D. Thomson, S. Wehmeier, F. J. Byfield, P. A. Janmey, D. Caballero-Lima, A. Crossley and A. C. Brand, *Cell. Microbiol.*, 2015, **17**, 342–354.
15 D. D. Thomson, J. Berman and A. C. Brand, *Fungal. Genet. Biol.*, 2016, **88**, 54–58.
16 A. Sanati Nezhad, M. Naghavi, M. Packirisamy, R. Bhat and A. Geitmann, *Lab Chip*, 2013, **13**, 2599–2608.
17 D. Felekis, H. Vogler, G. Mecja, S. Muntwyler, A. Nestorova, T. Huang, M. S. Sakar, U. Grossniklaus and B. J. Nelson, *Int. J. Rob. Res.*, 2015, **34**, 1136–1146.
18 N. Shamsudhin, N. Laeubli, H. B. Atakan, H. Vogler, C. Hu, W. Haeberle, A. Sebastian, U. Grossniklaus and B. J. Nelson, *PLOS ONE*, 2016, **11**, e0168138.
19 C. Hu, G. Munglani, H. Vogler, T. Ndinyanka Fabrice, N. Shamsudhin, F. K. Wittel, C. Ringli, U. Grossniklaus, H. J. Herrmann and B. J. Nelson, *Lab Chip*, 2017.
20 C. G. Agudelo, A. Sanati Nezhad, M. Ghanbari, M. Naghavi, M. Packirisamy and A. Geitmann, *Plant J.*, 2013, **73**, 1057–1068.
21 T. Geng, E. L. Bredeweg, C. J. Szymanski, B. Liu, S. E. Baker,

View Article Online
DOI: 10.1039/C7LC00725F

G. Orr, J. E. Evans and R. T. Kelly, *Sci. Rep.*, 2015, **5**, 16111.
22 M. Bastmeyer, H. B. Deising and C. Bechinger, *Annu. Rev. Biophys.*, 2002, **31**, 321–341.
23 A. Sanati Nezhad and A. Geitmann, *J. Exp. Bot.*, 2013, **64**, 4709–4728.
24 A. Sanati Nezhad, *Lab Chip*, 2014, **14**, 3262–3274.
25 A. Sanati Nezhad, M. Naghavi, M. Packirisamy, R. Bhat and A. Geitmann, *Proc. Natl. Acad. Sci. U.S.A.*, 2013, **110**, 8093–8098.
26 M. Gupta, L. Kocgozlu, B. R. Sarangi, F. Margadant, M. Ashraf and B. Ladoux, *Methods Cell Biol.*, 2015, **125**, 289–308.
27 A. Ghanbari, V. Nock, R. J. Blaikie, J. G. Chase, X. Chen, C. E. Hann and W. Wang, *Int. J. Comput. Appl. Tech.*, 2010, **39**, 137–144.
28 A. Ghanbari, V. Nock, S. Johari, R. J. Blaikie, X. Chen and W. Wang, *J. Micromech. Microeng.*, 2012, **22**, 095009.
29 S. Johari, V. Nock, M. M. Alkaisi and W. Wang, *Lab Chip*, 2013, **13**, 1699–1707.
30 V. Nock, A. B. Tayagui and A. Garrill, 19th International Conference on Miniaturized Systems for Chemistry and Life Sciences, pp. 692–694.
31 A. B. Tayagui, A. Garrill, D. Collings and V. Nock, 20th International Conference on Miniaturized Systems for Chemistry and Life Sciences, pp. 150–151.
32 W. C. Coker, *J. Elisha Mitchell Sci. Soc.*, 1927, **42**, 207–226.
33 L. Yang, X. Hao, C. Wang, B. Zhang and W. Wang, *Microsyst. Technol.*, 2014, **20**, 1933–1940.
34 J. Monahan, A. A. Gewirth and R. G. Nuzzo, *Anal. Chem.*, 2001, **73**, 3193–3197.
35 J. Schindelin, I. Arganda-Carreras, E. Frise, V. Kaynig, M. Longair, T. Pietzsch, S. Preibisch, C. Rueden, S. Saalfeld, B. Schmid, J.-Y. Tinevez, D. J. White, V. Hartenstein, K. Eliceiri, P. Tomancak and A. Cardona, *Nat. Meth.*, 2012, **9**, 676–682.
36 J.-Y. Tinevez, N. Perry, J. Schindelin, G. M. Hoopes, G. D. Reynolds, E. Laplantine, S. Y. Bednarek, S. L. Shorte and K. W. Eliceiri, *Methods*, 2017, **115**, 80–90.
37 S. Johari, H. Fazmir, A. F. M. Anuar, M. Z. Zainol, V. Nock and W. Wang, 2015 IEEE Regional Symposium on Micro and Nanoelectronics (RSM), pp. 1–4.
38 J. C. McDonald, D. C. Duffy, J. R. Anderson, D. T. Chiu, H. Wu, O. J. A. Schueller and G. M. Whitesides, *Electrophoresis*, 2000, **21**, 27–40.
39 K. K. Lee, L. Labiscsak, C. H. Ahn and C. I. Hong, *Fungal. Genet. Biol.*, 2016, **94**, 11–14.
40 L. J. McKerracher and I. B. Heath, *Exp. Mycol.*, 1987, **11**, 79–100.
41 A. Muralidhar, E. Swadel, M. Spiekerman, S. Suei, M. Fraser, M. Ingerfeld, A. B. Tayagui and A. Garrill, *Microbiology*, 2016, **162**, 206–213.
42 J. Mark, *Polymer Data Handbook*, Oxford University Press, 2009.
43 J. Koh, J. Kim, J. H. Shin and W. Lee, *Appl. Phys. Lett.*, 2014, **105**, 114103.
44 I. Schoen, W. Hu, E. Klotzsch and V. Vogel, *Nano Lett.*, 2010, **10**, 1823–1830.
45 S. Johns, C. M. Davis and N. P. Money, *Microbiol. Res.*, 1999, **154**, 225–231.
46 R. R. Lew, N. N. Levina, S. K. Walker and A. Garrill, *Fungal. Genet. Biol.*, 2004, **41**, 1007–1015.
47 N. P. Money, C. M. Davis and J. P. Ravishankar, *Fungal. Genet. Biol.*, 2004, **41**, 872–876.
48 D. L. Delgado-Alvarez, O. A. Callejas-Negrete, N. Gomez, M. Freitag, R. W. Roberson, L. G. Smith and R. R. Mourino-Perez, *Fungal. Genet. Biol.*, 2010, **47**, 573–86.

View Article Online
DOI: 10.1039/C7LC00725F

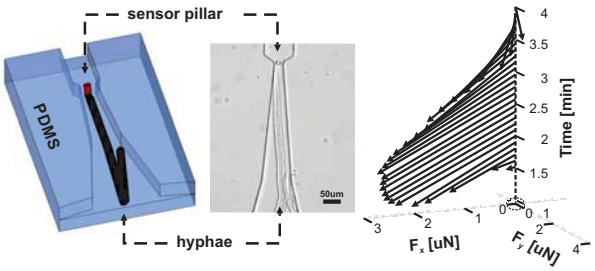

We introduce a platform capable of quantifying magnitude and direction of protrusive forces exerted by individual tips of hyphal microorganisms using elastomeric micropillars.